TU Delft

Delft University of Technology

Investigation on the melting of the weld interface in continuous ultrasonic welding of thermoplastic composites

Jongbloed, Bram; Teuwen, Julie J.E.; Fernandez Villegas, Irene; Benedictus, Rinze

Publication date
2019

Document Version
Final published version

Published in
Proceedings of 22nd International Conference on Composite Materials (ICCM), Melbourne (Australia), 2019

Citation (APA)
Jongbloed, B., Teuwen, J. J. E., Fernandez Villegas, I., & Benedictus, R. (2019). Investigation on the melting of the weld interface in continuous ultrasonic welding of thermoplastic composites. In *Proceedings of 22nd International Conference on Composite Materials (ICCM), Melbourne (Australia), 2019*

Important note
To cite this publication, please use the final published version (if applicable).
Please check the document version above.

Copyright
Other than for strictly personal use, it is not permitted to download, forward or distribute the text or part of it, without the consent of the author(s) and/or copyright holder(s), unless the work is under an open content license such as Creative Commons.

Takedown policy
Please contact us and provide details if you believe this document breaches copyrights.
We will remove access to the work immediately and investigate your claim.

This work is downloaded from Delft University of Technology.
For technical reasons the number of authors shown on this cover page is limited to a maximum of 10.

INVESTIGATION ON THE MELTING OF THE WELD INTERFACE IN CONTINUOUS ULTRASONIC WELDING OF THERMOPLASTIC COMPOSITES

Bram Jongbloed[1], Julie Teuwen[2], Irene Fernandez Villegas[3], and Rinze Benedictus[4]

[1]Aerospace Manufacturing Technologies, Faculty of Aerospace Engineering, Delft University of Technology, Kluyverweg 1, 2629 HS Delft, The Netherlands,
email: B.C.P.Jongbloed@tudelft.nl, website: www.tudelft.nl
[2]Aerospace Manufacturing Technologies, Faculty of Aerospace Engineering, Delft University of Technology, Kluyverweg 1, 2629 HS Delft, The Netherlands,
email: J.J.E.Teuwen@tudelft.nl, website: www.tudelft.nl
[3]Aerospace Manufacturing Technologies, Faculty of Aerospace Engineering, Delft University of Technology, Kluyverweg 1, 2629 HS Delft, The Netherlands,
email: I.FernandezVillegas@tudelft.nl, website: www.tudelft.nl
[4]Structural Integrity & Composites, Faculty of Aerospace Engineering, Delft University of Technology, Kluyverweg 1, 2629 HS Delft, The Netherlands,
email: R.Benedictus@tudelft.nl, website: www.tudelft.nl

Keywords: Fusion bonding, Energy director, Polymer mesh, High frequency welding, Joining

ABSTRACT

Continuous ultrasonic welding is a new promising high-speed joining technique for thermoplastic composites. At the moment no straightforward method exists to find an optimum welding speed to easily obtain high strength joints. However, for static ultrasonic welding a systematic approach is available. Therefore, the aim of this study is to understand whether the optimum welding time in static ultrasonic welding can be related to the welding speed in continuous ultrasonic welding. The duration of the welding stages in static and continuous welding were compared in order to find similarities and discrepancies. The duration of the welding stages in continuous ultrasonic welding was estimated by analysing the weld interface and measuring the distances of the stages in the fractured interface around the location where the weld was stopped. No significant difference in weld duration was found for the first welding stage in which the mesh energy director is flattened. However, the second stage in which the energy director and adherends melt simultaneously, lasted much longer for the continuous welding process. This was possibly caused by the more constraining boundary conditions in the continuous welding process. In conclusion, the optimum welding speed in continuous welding was lower than the expected optimum welding speed based on the optimum welding time in static ultrasonic welding, because the second welding stage lasted longer in the continuous ultrasonic welding process.

1 INTRODUCTION

Carbon fibre-reinforced thermoplastic composites are gaining interest for the manufacturing of primary and secondary structures for the next generation aircraft. The main reasons are the ease of manufacturing (e.g. hot press forming), the high material toughness, the recyclability of entire components and scraps produced during manufacturing, and the possibility to weld the thermoplastic composite components together. These reasons contribute to lowering the manufacturing costs of aircraft.

The usage of resistance welding to assemble the fixed leading edge of the A380 [1], and the usage of induction welding to assemble the rudder and elevators of the Gulfstream G650 [2], demonstrate the applicability of welding techniques in the aerospace industry. Another welding technique that has not been applied industrially yet is ultrasonic welding. This technique is very fast, energy efficient, and can potentially been monitored and controlled in situ. Especially with the expectation that for next generation aircraft large structural components will be made from thermoplastic composites, the need for a high speed, and thus low-cost welding technique increases.

During the ultrasonic welding process a horn (called sonotrode) exerts high frequency, low amplitude vibrations to the welding stack, while at the same time applying a static force. These vibrations heat up the interface through frictional and viscoelasic heating. In order to focus the heat generation at the interface a thin resin rich layer, called an energy director is used [3, 4]. The low-stiffness energy director experiences a higher cyclic strain due to the vibrations and therefore heats up faster than the adherends. For the continuous welding process this sonotrode slides over the to-be-welded overlap, while it applies the mechanical vibrations and static welding force [5].

Most research in the field of ultrasonic welding of thermoplastic composites focuses on static welding [3, 4, 6–12] and spot welding [13, 14]. Villegas at al. showed that during the static welding process different stages can be identified corresponding to heating up and melting of the weld interface [6]. The feedback data (power and vertical sonotrode displacement) from the welder could be used to in situ monitor and control the welding process [3, 7]. Villegas et al. showed that by identifying where the stages occur in the welding process, it is possible to find optimum welding conditions that consistently result in high strength joints [3, 7].

Continuous ultrasonic welding has been shown to be a promising high speed welding technique for CF/PPS (carbon fibre-reinforced polyphenylene sulfide) thermoplastic composites. Senders et al. demonstrated the possibility of welding two composites plates together by using zero-flow welding with a thin energy director at the interface to focus the heat generation [5]. We continued with the same composite material and experimental setup and showed that the weld uniformity and quality could be improved by using a woven polymer mesh as energy director [15]. In contrast with static ultrasonic welding, no knowledge is available on identifying optimum welding conditions in a systematic way for continuous ultrasonic welding. For static welding, the welding stages happen one after the other for the entire interface, which makes it possible to use the machine feedback data to identify optimum welding conditions to control the process. While for the continuous welding process a part of the weld interface continuously transitions from not welded, i.e. pristine energy director, to fully welded as demonstrated in Figure 1, which implies that if weld stages could be identified in continuous ultrasonic welding they will be present at the weld interface simultaneously. Therefore, the machine feedback data in continuous ultrasonic welding will not show the individual weld stages. An easy way to be able to find optimum welding conditions for continuous ultrasonic welding, would be to translate the optimum welding time from static welding into an optimum welding speed in continuous ultrasonic welds.

Therefore, the aim of this study is to understand whether the optimum welding time in static ultrasonic welding can be related to the welding speed in continuous ultrasonic welding. In order to understand whether a correlation exists, the melting of the weld interface in continuous ultrasonic welding was studied by analysing the fracture surface of the area under the sonotrode of welds stopped before the entire seam was welded. The melting duration of the weld interface was estimated based on the fracture surfaces and compared to the welding time in static welding.

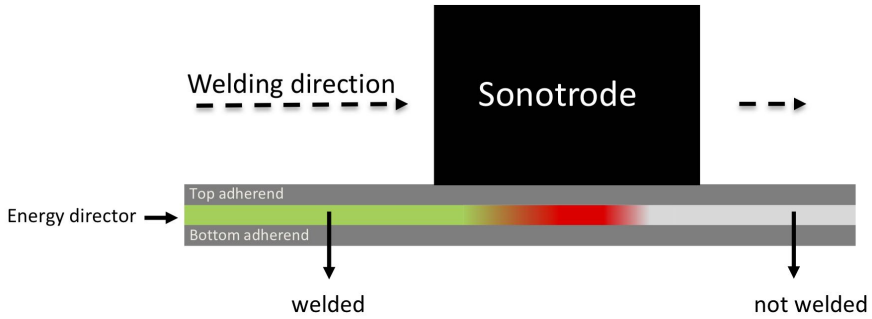

Figure 1: Schematic side view of weld interface during the continuous ultrasonic welding process. Not welded director shown ahead of the sonotrode, a hot area under the sonotrode, and a welded area behind the sonotrode.

2 METHODS

2.1 Materials

The thermoplastic composite laminates used for the welding experiments in this study were made from carbon fibre-reinforced polyphenylene sulfide (CF/PPS) fabric (five harness satin weave). The product code of this semi-preg material is CF 0286 127 Tef4 43% (TenCate Advanced Composites, the Netherlands). The laminates were stacked according to $[0/90]_{3s}$ sequence, and consolidated in a hot plate press for 20 min at 320°C and 1 MPa pressure. The consolidated laminates had a size of 580 mm by 580 mm, and a thickness of 1.85 mm. 220 mm by 101.6 mm adherends were cut from the consolidated laminates for the continuous welding process. For the static welding process 25.4 mm by 101.6 mm coupons were cut from the laminates. A 0.20 mm-thick woven polymer mesh energy director was used for all experiments to focus the heat generation to the interface [15]. The energy director had product name PPS100 and was supplied by PVF GmbH, Germany.

2.2 Static ultrasonic welding process

The static welding setup is shown in Figure 2. A custom-built jig kept the coupons in place ensuring an overlap of 12.7 mm. The spring supported platform in Figure 2a minimised potential bending by allowing vertical displacement of the upper coupon. Figure 2b shows a side view of the overlapping coupons (black) together with the energy director (grey).

The ultrasonic welder was a VE20 Slimline dialog 6200 from Herrmann Ultrasonics. The welding train within the machine consisted of a 20 kHz converter, booster, and sonotrode. The converter had a maximum peak-to-peak amplitude of 26.6 μm. The booster had a gain of 2 and the sonotrode a gain of 1.6. The rectangular sonotrode had a contact surface of 15 mm by 30 mm, which made it possible to fully cover the 12.7 mm by 25.4 mm overlap. The welding machine recorded the consumed power [W], vertical sonotrode displacement [mm], and welding force [N] at a rate of 1 kHz during the welding process. This data was called feedback data. The corresponding graphs from this data were called weld curves.

Different experiments with two different welding forces were used, since the welding force is known to have a significant influence on the optimum welding time [6]. The optimum welding time was defined as the welding time required to obtain a high strength weld. Villegas' method-

ology was used to identify the optimum welding time [3]. The used welding forces were 500 N and 1500 N. The peak-to-peak amplitude of the vibrations was fixed to 80 μm. For each parameter set (500 N, 80 μm, and 1500 N, 80 μm) three static welds were made and an average duration for the welding stages (i.e. the flattening of the mesh during the initial displacement, and the simultaneous melting of the energy director and adherends during the displacement plateau) was calculated. In order to obtain the full weld curves, displacement controlled welding was used with a displacement value of 0.20 mm.

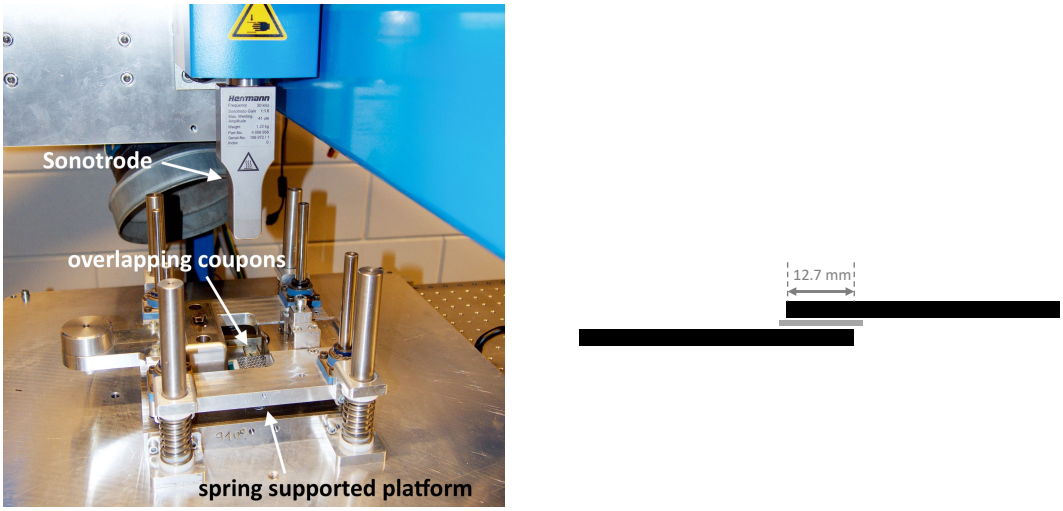

(a) (b)

Figure 2: (a) Static ultrasonic welding setup with an in-house built welding jig for single lap shear coupons. (b) Shows how the coupons overlap each other. The grey line represents the energy director in between the black adherends.

2.3 Continuous ultrasonic welding procedure

The same ultrasonic welder, sonotrode, welding forces, and welding amplitude as for the static welds were used for continuous ultrasonic welding. The ultrasonic welder was a VE20 Slimline dialog 6200 from Herrmann Ultrasonics. The welding train within the machine consisted of a 20 kHz converter, booster, and sonotrode. The converter had a maximum peak-to-peak amplitude of 26.6 μm. The booster had a gain of 2 and the sonotrode a gain of 1.6. For the continuous welding experiments an in-house built continuous ultrasonic welding machine, shown in Figure 3a, was used. During the welding process the sonotrode moved over the overlapping top and bottom adherends while exerting a static welding force and transverse mechanical ultrasonic vibrations (Figure 3b). The X-Y table could move automatically in X-direction during the welding process. On top of the X-Y table a fixture was placed holding the to-be-welded adherends. A steel support plate plate was placed under the top adherend with a thickness equal to the adherend thickness (1.85 mm). The adherends were kept in place by two bar clamps. The distance between the clamps was 70 mm. Alignment pins were used to ensure proper alignment of the adherends. The pins were placed such that the overlap between the top and bottom adherend was 12.7 mm.

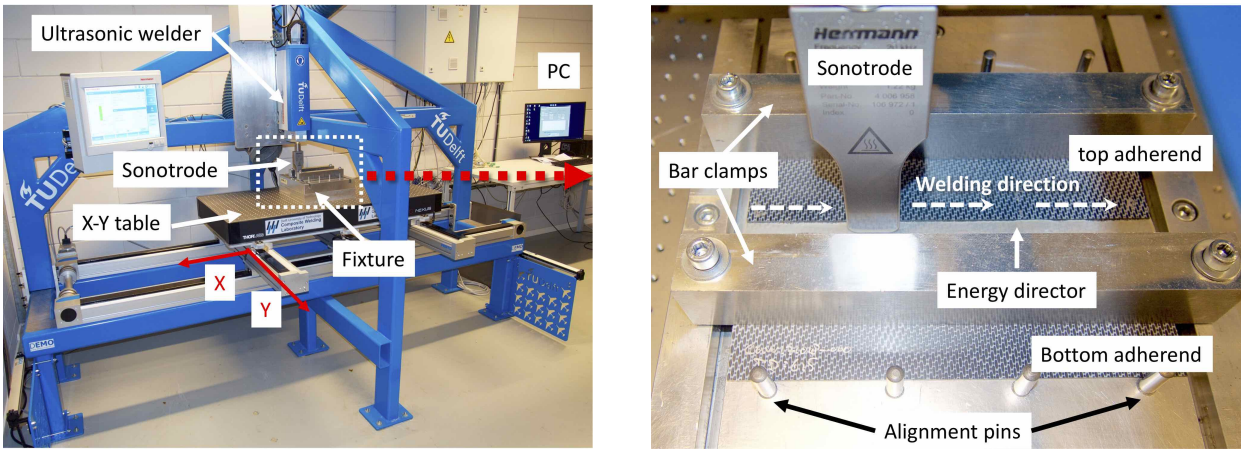

(a) (b)

Figure 3: (a) Overview of the continuous ultrasonic welding machine. (b) A closer view of the welding setup and clamping.

2.4 Experimental techniques

For continuous ultrasonic welding the welding speed that resulted in the highest strength was called optimum welding speed. In order to find the optimum continuous welding speed, different welding speeds (25 mm/s, 35 mm/s, 45 mm/s, and 55 mm/s) were used for the parameter sets (500 N, 80 μm, and 1500 N, 80 μm) by fully welding a 220 mm-long seam. After the welding process six 25.4 mm-wide single lap shear samples were cut from each set of welded adherends after discarding the two edges. The welded single-lap shear samples were mechanically tested with a Zwick/Roell 250 kN universal testing machine with a cross-head speed of 1.3 mm/min according to ASTM D 1002. The grips were given the necessary offset to ensure parallelism between the load introduction and the overlap.

To be able to visualise the weld interface for the continuous welding process, the welding process was stopped before the entire seam was welded. The process was stopped after welding 56 mm, 100 mm, and 144 mm with respect to the starting point that was 7.5 mm from the edge of the overlapping plates and coincided with the middle of the sonotrode. A 50 mm-wide lap shear coupon was cut around each stopped welding location. After lap shear testing the coupon, the obtained fracture surfaces were analysed using a ZEISS Discovery.V8 SteREO microscope.

3 RESULTS

3.1 Welding stages in static welding

Static ultrasonic welds were made in order to identify and obtain the duration of the individual welding stages and the optimum welding time for the static welding process. Figure 4 shows representative power and displacement curves for the static welds made with a welding force of 500 N and 1500 N. The displacement curves increased steeply at the beginning of the welding process (A to B) when the mesh was being flattened [15] until a displacement plateau was reached (B to C). From the start of the displacement plateau both the energy director and the adherends were melting simultaneously [15]. After this plateau the displacement further increased. Following the method from Villegas et al. [3,6] the optimum welding time for the mesh energy director could be

found at the end of the displacement plateau [15]. The estimated optimum welding times, i.e. A-C duration, were apprximately 295 ms and 151 ms for 500 N and 1500 N welding force, respectively. The duration of stage A-B (199 ms) (Figure 4a) for a 500 N welding force was significantly longer compared to the duration of stage A-B (63 ms) (Figure 4b) for a welding force of 1500 N. Stage B-C was found to be very similar for both welding forces: 96 ms for a 500 N welding force (Figure 4a) and 88 ms for a welding force of 1500 N (Figure 4b).

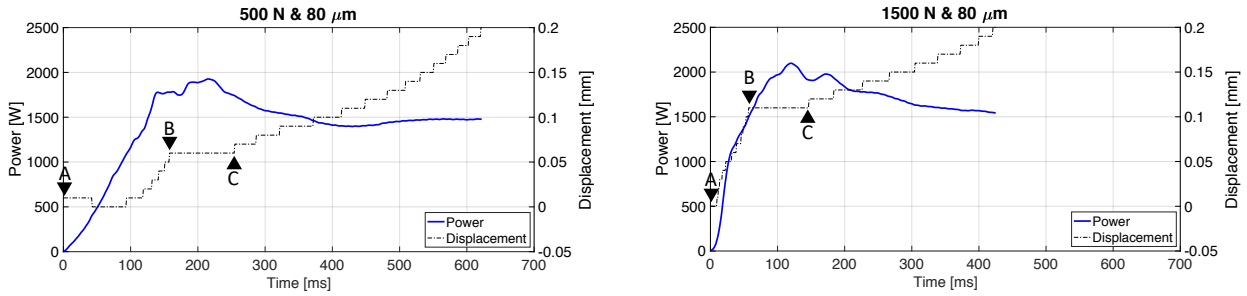

(a) (b)

Figure 4: Representative power and displacement curves for (a) 500 N (b) 1500 N welding force and 80 μm amplitude of the vibrations. The stages A-B and B-C have been indicated. During stage A-B the mesh energy director was being flattened and during stage B-C the energy director and the adherends were melting simultaneously [15].

3.2 Melting of the weld interface in continuous ultrasonic welding

In order to visualise the melting of the weld interface in the continuous ultrasonic welding process, the process was stopped before the entire seam was welded for different welding speeds and two different welding forces.

3.2.1 Welding stage A-B

Figure 5a shows a representative fracture surface at and around the location where the sonotrode was stopped of a continuous weld made with a welding force of 500 N. The white dashed rectangle at the weld interface represents the position of the sonotrode at the moment the welding process was stopped. The direction in which the sonotrode moved with respect to the adherends is also indicated. On the right in Figure 5a, the energy director is distinctly present, while on the left the energy director became significantly less distinct. This transition was indicated by location B, related to moment B in static ultrasonic welding, where not only the mesh energy director, but also the adherends started melting. Location B was found not to coincide with the right edge of the sonotrode. In Figure 5b a part of the fracture surface ahead of location B was enlarged. It could be observed that another transition took place where the energy director changes from pristine to partially flattened, denoted as location A. Thus, stage A-B was identified during which the energy director was being flattened.

The distance between location A and B could be measured in the fracture surfaces for the different welding speeds and forces. These measured distances could be converted into a duration by dividing the distances by the welding speeds. The obtained duration for stage A-B in continuous welding could then be compared to the duration of stage A-B in static welding. Figure 6 shows the time that stage A-B lasted for the continuous and for the static welding process (0 mm/s). The

duration of stage A-B for the continuous welds was found to be close to the duration of stage A-B for the static welds. Additionally, the duration of stage A-B for the continuous welding process did not change for the different welding speeds.

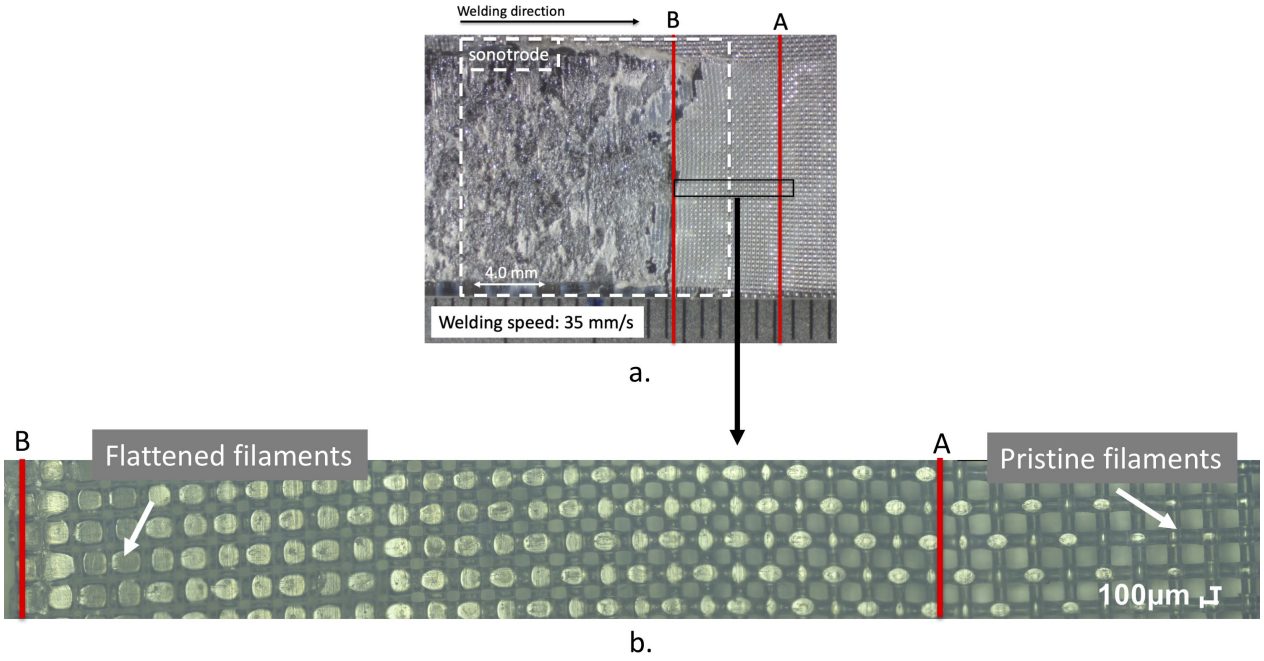

Figure 5: (a.) Representative partial fracture surface of a weld stopped during the welding process before the entire seam was welded for a welding force of 35 mm/s. (b.) The flattening of the mesh between A-B is shown. A 500 N welding force and a vibrational amplitude of 80 μm were used.

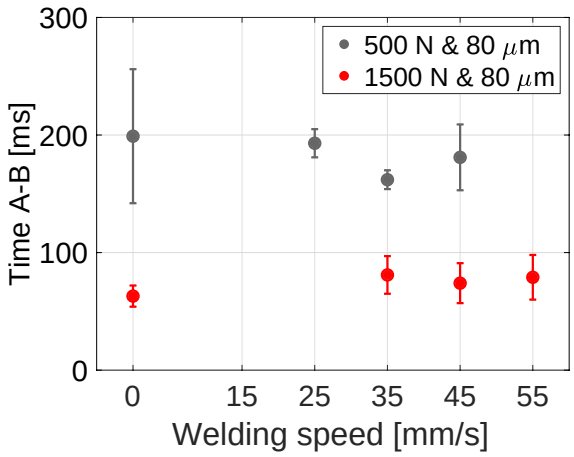

Figure 6: Time that stage A-B lasted for static (0 mm/s) and continuous welding. Error bars indicate the standard deviation (n=3).

Figure 7 shows two representative fracture surfaces of continuous welds: one weld made with a welding force of 1500 N and a welding speed of 35 mm/s, and one weld made with a welding force of 500 N and a welding speed of 45 mm/s. The welding force and respectively the welding speed

were increased as compared to the welding force and welding speed of the weld shown in Figure 5. In Figure 7a the distance between A-B decreased compared to Figure 5a when the welding force was increased from 500 N to 1500 N. Location B, where the adherends started melting, moved towards the front edge of the sonotrode. In Figure 7b the distance between A-B increased when the welding speed was increased with 10 mm/s compared to Figure 5a. Location B moved towards the middle of the sonotrode, which resulted in a significantly larger distance between A-B.

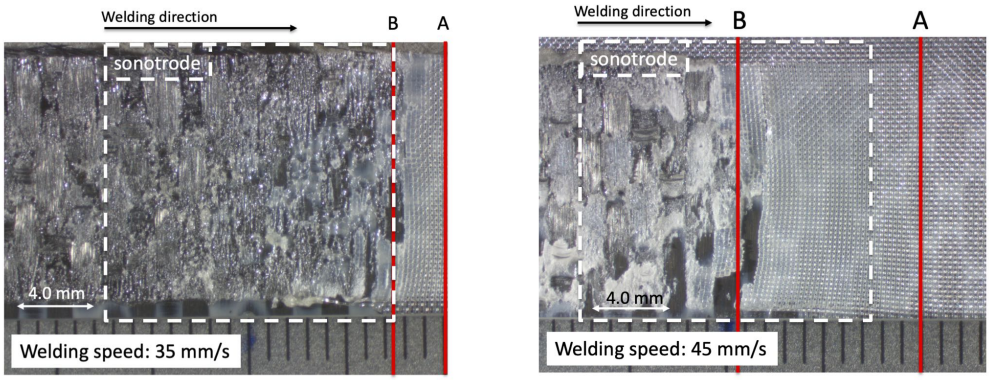

Figure 7: Representative partial fracture surfaces of two welds stopped during the welding process for (a.) a welding speed of 35 mm/s, welding force of 1500 N, a welding amplitude of 80 μm, and (b.) a welding speed of 45 mm/s, a welding force of 500 N, a welding amplitude of 80 μm. The white dashed rectangular box indicates the location where the sonotrode stopped.

3.2.2 Welding stage B-C

In static welding the flattening of the mesh in stage A-B was followed by stage B-C as seen in Figure 4. In order to compare the duration of stage B-C in continuous welding to the duration of stage B-C in static welding, it was needed to determinate where moment C occurred. For the static welding process moment C indicated the optimum welding time [15]. It can be expected that in continuous ultrasonic welding moment C coincided with the rear edge of the sonotrode in optimum welding conditions (i.e. optimum welding speed) as indicated in Figure 8. Therefore, only the optimum welding speeds were used to determine stage B-C.

To find an optimum welding speed for the two welding forces, three welding speeds per welding force were used. Figure 9 shows the average lap shear strength for different welding speeds. It could be observed that the highest lap shear strength with a welding force of 500 N was obtained with the optimum welding speed of 35 mm/s, while for a welding force of 1500 N the highest lap shear strength was obtained for an optimum welding speed of 45 mm/s.

Figure 10 shows the time that stage B-C lasted for the static (0 mm/s) and for the continuous welding process. It could be observed that the difference in duration of stage B-C for the two welding forces was negligible with a difference of approximately 20 ms for the continuous process. However, when comparing the time of stage B-C for the continuous process to the static process a large difference was found. The duration of stage B-C during the continuous welding process was approximately 3 to 3.5 times higher as compared the the same stage during the static welding process.

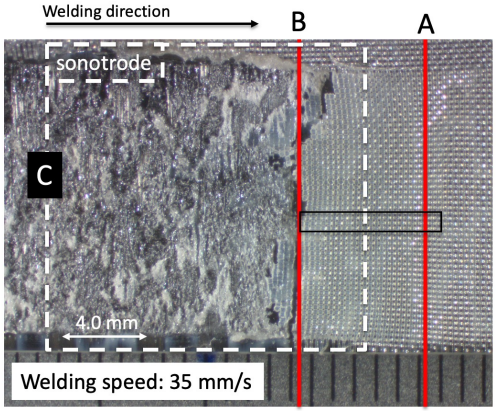

Figure 8: Representative partial fracture surface a weld stopped during the welding process before the entire seam was welded for the optimum welding speed 35 mm/s. A 500 N welding force and a vibrational amplitude of 80 μm were used. Stages A-B, and B-C have been indicated.

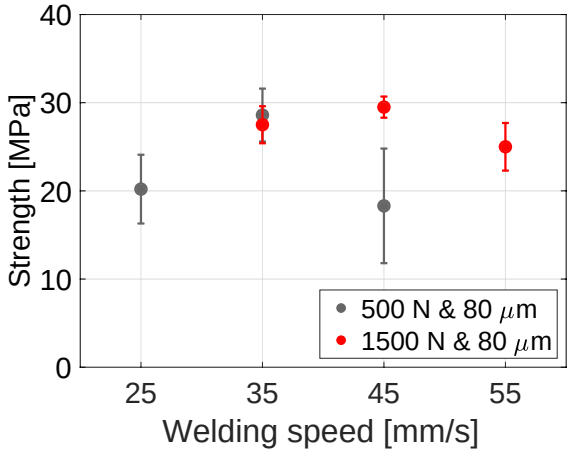

Figure 9: Lap shear strength obtained for different welding speeds for a 500 N and 1500 N welding force and an amplitude of vibration of 80 μm. The error bars indicate the standard deviation (n=6).

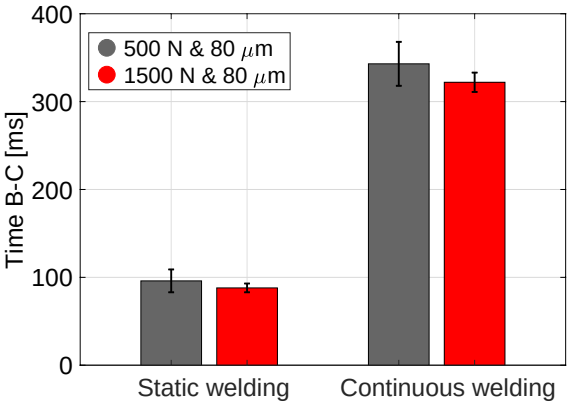

Figure 10: Duration of stage B-C for static and continuous welding. For the continuous welds the optimum welding speed 35 mm/s for a welding force of 500 N and the optimum welding speed 45 mm/s for a welding force of 1500 N were used. Error bars indicate the standard deviation (n=3).

4 DISCUSSION

If it were possible to directly relate the optimum welding time in static welding to continuous welding then the optimum welding speeds could be logically estimated by dividing the width of the sonotrode by the optimum welding time in static welding. Two different optimum welding times were obtained in the static welding process for the two welding forces. This would result in a welding speed of 50 mm/s for a welding force of 500 N and a welding speed of 100 mm/s for a welding force of 1500 N. However, Figure 9 shows that the optimum welding speeds that give the highest strength are approximately 1.4 to 2.2 times lower than the calculated speeds. Thus a direct translation of optimum welding time to optimum welding speed is not straightforward.

Because a direct translation from the static to the continuous process is not straightforward, we will now focus on the individual welding stages in order to understand why this direct translation is not possible. The welding stages identified in static welding for the energy directing mesh are also observed in the continuous welding process. The main difference is that for continuous welding all the stages of the process are present at the interface simultaneously. The duration of the A-B welding stage seems to be independent of the welding speed. The duration of the first stage A-B in static and continuous welding are similar. Thus the discrepancy between the expected optimum welding speeds and the actual optimum welding speeds does not come from the initial welding stage A-B. As expected the welding force had a significant influence on the duration of stage A-B. By increasing the welding force from 500 N to 1500 N the duration was reduced three times. Most likely the heat generation in this stage mainly relies on surface friction. Therefore it is logical that by increasing the welding force the duration of stage A-B reduces since the friction increases.

For stage B-C, the duration of the static and continuous process is very different. Stage B-C lasts approximately 3 to 3.5 times longer in the continuous welding process. Thus the difference between the expected optimum welding speed translated from the static welding process and the actual optimum welding speed originates from this stage. Possibly different heating rates exist for the static and the continuous welding process. The continuous welding process might have a lower heating rate due to different boundary conditions. It seems that increasing the welding force from 500 N to 1500 N does not have an influence on the duration of stage B-C for both the static and the continuous process.

5 CONCLUSION

The aim of this paper is to understand how the optimum welding time in static ultrasonic welding is related to the optimum welding speed in continuous ultrasonic welding. It was found that a direct translation of the optimum welding time in static welding to an optimum welding speed in continuous ultrasonic welding is not straightforward. The duration of the two main welding stages in static and continuous welding were compared, i.e. the stage in which the energy director is being flattened and the stage in which the adherends and the energy director melt simultaneously. The duration of the first stage, in which the mesh energy director flattens, was found to be similar for both static and continuous welding. However, the duration of the consecutive stage, in which the adherends and mesh melt simultaneously, was found to last approximately 3 to 3.5 longer for the continuous process. When it is understood why the last welding stage lasts longer in continuous welding as compared to static welding, then it might be possible to directly translate the optimum welding time in static welding to an optimum welding speed in continuous welding.

ACKNOWLEDGEMENTS

This study was funded by the European research programme Clean Sky. The ecoTECH project has received funding from the European Unions Horizon 2020 Clean Sky 2 Joint Undertaking under the AIRFRAME ITD grant agreement 807083.

REFERENCES

[1] G. Gardiner. Thermoplastic composites gain leading edge on the A380. *High-Performance Composites*, 14(2):50–55, 2006.

[2] Arnt Offringa. New thermoplastic composite design concepts and their automated manufacture. *JEC composites magazine*, 58:45–49, 2010.

[3] I.F. Villegas. In situ monitoring of ultrasonic welding of thermoplastic composites through power and displacement data. *Journal of Thermoplastic Composite Materials*, 28(1):66–85, 2015.

[4] G. Palardy and I.F. Villegas. On the effect of flat energy directors thickness on heat generation during ultrasonic welding of thermoplastic composites. *Composite Interfaces*, 24(2):203–214, 2017.

[5] F. Senders, M. van Beurden, G. Palardy, and I.F. Villegas. Zero-flow: A novel approach to continuous ultrasonic welding of CF/PPS thermoplastic composite plates. *Advanced Manufacturing: Polymer & Composites Science*, 0340(September 2017):1–10, 2016.

[6] I.F. Villegas. Strength development versus process data in ultrasonic welding of thermoplastic composites with flat energy directors and its application to the definition of optimum processing parameters. *Composites Part A: Applied Science and Manufacturing*, 65:27–37, 2014.

[7] I.F. Villegas, B. Valle Grande, H.E.N. Bersee, and R. Benedictus. A comparative evaluation between flat and traditional energy directors for ultrasonic welding of cf/pps thermoplastic composites. *Composite Interfaces*, 22(8):717–729, 2015.

[8] I.F. Villegas and P.V. Rubio. On avoiding thermal degradation during welding of high-performance thermoplastic composites to thermoset composites. *Composites Part A: Applied Science and Manufacturing*, 77(Supplement C):172 – 180, 2015.

[9] A. Levy, S. Le Corre, and I.F. Villegas. Modeling of the heating phenomena in ultrasonic welding of thermoplastic composites with flat energy directors. *Journal of Materials Processing Technology*, 214(7):1361–1371, 2014.

[10] I.F. Villegas and H. Bersee. Ultrasonic welding of advanced thermoplastic composites: An investigation on energy-directing surfaces. *Advances in Polymer Technology*, 29(2):112–121, 2010.

[11] W. Tao, X. Su, H. Wang, Z. Zhang, H. Li, and J. Chen. Influence mechanism of welding time and energy director to the thermoplastic composite joints by ultrasonic welding. *Journal of Manufacturing Processes*, 37:196–202, 2019.

[12] K. Goto, K. Imai, M. Arai, and T. Ishikawa. Shear and tensile joint strengths of carbon fiber-reinforced thermoplastics using ultrasonic welding. *Composites Part A: Applied Science and Manufacturing*, 116:126–137, 2019.

[13] T. Zhao, G. Palardy, I.F. Villegas, C. Rans, M. Martinez, and R. Benedictus. Mechanical behaviour of thermoplastic composites spot-welded and mechanically fastened joints: A preliminary comparison. *Composites Part B: Engineering*, 112:224–234, 2017.

[14] T. Zhao, C. Broek, G. Palardy, I.F. Villegas, and R. Benedictus. Towards robust sequential ultrasonic spot welding of thermoplastic composites: Welding process control strategy for consistent weld quality. *Composites Part A: Applied Science and Manufacturing*, 109:355–367, 2018.

[15] B.C.P. Jongbloed, J.J.E. Teuwen, Genevieve Palardy, and Irene Fernandez Villegas. Improving weld uniformity in continuous ultrasonic welding of thermoplastic composites. *ECCM18: 18th European Conference on Composite Materials*, (June):24–28, 2018.